Reprinted from

CMES

Computer Modeling in Engineering & Sciences

Founder and Editor-in-Chief:
Satya N. Atluri

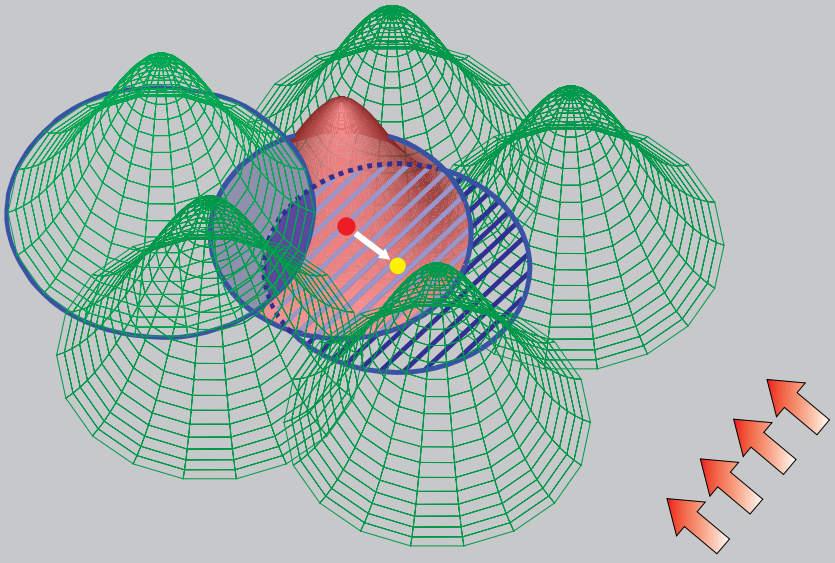

ISSN: 1526-1492 (print)
ISSN: 1526-1506 (on-line)

Tech Science Press

 CMES, vol.78, no.4, pp.225-245, 2011

Numerical Design of Random Micro-Heterogeneous Materials with Functionally-Graded Effective Thermal Conductivities Using Genetic Algorithms and the Fast Boundary Element Method

Marco Dondero[1], **Adrián P. Cisilino**[1,2] **and J. Pablo Tomba**[1]

Abstract: This paper introduces a numerical methodology for the design of random micro-heterogeneous materials with functionally graded effective thermal conductivities (ETC). The optimization is carried out using representative volume elements (RVEs), a parallel Genetic Algorithm (GA) as optimization method, and a Fast Multipole Boundary Element Method (FMBEM) for the evaluation of the cost function. The methodology is applied for the design of foam-like microstructures consisting of random distributions of circular insulated holes. The temperature field along a material sample is used as objective function, while the spatial distribution of the holes is the design variable. There are presented details of the FMBEM and the GA implementations, their customizations and tune up, and the analysis for the sizing of the RVE. The effectiveness of the proposed methodology is demonstrated for two examples. Computed results are experimentally validated using ad-hoc devised experiments.

Keywords: Effective thermal conductivity, random composites, Fast Multipole Boundary Element Method, homogenization, representative volume element, functionally graded materials.

1 Introduction

Effective thermal conductivity (ETC) of micro-heterogeneous materials is an active research field as it has been for over a century. The importance of micro-heterogeneous materials like granular metal and ceramics, or polymeric open-cell foams lies in their applications in high performance insulation, packed beds, heterogeneous catalysts, composite materials and powder metallurgy. The size, shape,

[1] INTEMA, Faculty of Engineering, University of Mar del Plata-CONICET. Av. Juan B. Justo 4302, Mar del Plata, Argentina
[2] Corresponding author, email: cisilino@fi.mdp.edu.ar

physical properties and spatial distribution of the micro-structural constituents largely determine the macroscopic, overall behavior of these multi-phase materials. From the point of view of materials design, it would be highly attractive to tailor the material microstructure in order to obtain the desired set of macroscopic properties. One remarkable example of this concept can be found in the so-called Functionally Graded Materials (FGM). FGMs are composite materials formed of two or more constituent phases with a continuously variable composition. They are usually associated with particulate composites where the volume fraction of particles varies in one or several directions [Birman and Byrd, 2007].

In general, homogenized models based on the Mori–Tanaka and the self-consistent methods, i.e., the locally heterogeneous nature of FGM is disregarded [Birman and Byrd, 2007]. Homogenized models allow for the solution of heat transfer in FGMs. In particular, boundary element formulations for the solution of transfer in FGMs have been proposed, among others, by Chen et al [2002], Sladek et al [2003] and Sutradahar and Paulino [2003] and Paulino et al [2005].

Optimization problems are natural for FGM design, due to the possibility they offer to combine dissimilar materials throughout the structure [Birman and Byrd, 2007]. Computational modeling of the material microstructure together with homogenization techniques are widely used to predict the macroscopic behavior of random heterogeneous materials [Zohdi and Wriggers, 2005]. The homogenization of microstructures with randomly distributed components uses statistically representative volume elements (RVE). In order to make the material simulated data reliable, the RVE must be small enough to be considered as a material point with respect to the size of the domain under analysis, but large enough to be a sample statistically representative for the microstructure. Thus, a RVE usually contains a large number of heterogeneities, and therefore the computations could be expensive.

It is presented in this paper a numerical procedure for the design of random micro-heterogeneous materials with functionally-graded effective thermal conductivities. The methodology is devised for the design of foam-like microstructures consisting of random distributions of circular insulated holes. The temperature field along a material sample is used as objective function, while the spatial distribution of the holes is the design variable. Optimization is performed using a Genetic Algorithm (GA). GAs have the ability to overcome the difficulties due to objective function nonconvexity and lack of regularity characterizing the constrained design of random particulate media [Zohdi and Wriggers, 2005]. GAs simulate the natural evolution of species making use of the genetic operators. These are natural selection, pairing and mutation. Individuals live in an environment determined by the objective (or fitness) function, where they compete for survival and only the best ones success. The components of individuals are the chromosomes, the ge-

netic material that dictates unique properties of the individuals [Goldberg 1999]. Genetic Algorithms are robust global optimizers but they have high computational cost due to the repetitive evaluation of the fitness function. Moreover, and as it will be shown in the following sections, the evaluation of the fitness function for this work requires the solution of the temperature field for computationally expensive models containing large number of voids.

The Boundary Element Method (BEM) was selected as the analysis tool for this work due to simplicity in the generation of the model data (the model discretization is restricted only to the boundaries) and its superior accuracy when compared to other methods [Aliabadi and Wrobel 2002]. Moreover, bearing in mind the high computational demands of the genetic algorithm, the BEM was implemented using a fast multipole approach, the so-called Fast Multipole Boundary Element Method (FMBEM). The FMBEM reduces the computational cost of the direct BEM, from an order of $O(N^3)$ to a quasi-linear, where N is the number of degrees of freedom of the model. This reduction is achieved by multilevel clustering of the boundary elements into cells, the use of the multipole series expansion for the evaluation of the fundamental solutions in the far field, and the use of an efficient iterative solver. Additionally, the multipole algorithm leads to a matrix-free calculation scheme what results in a drastic reduction in the memory storage requirements.

The paper presents the details of the FMBEM and the GA implementations, their customizations and tuning-ups to deal with foam-like microstructures, and the analysis for the sizing of the RVE. The effectiveness of the proposed methodology is demonstrated for two examples. Computed results are experimentally validated using ad-hoc devised experiments.

2 The Fast Multipole Boundary Element Method and Modeling Considerations

The FMBEM implemented for this work follows that introduced by Liu and Nishimura [2006]. The FMBEM was tailored to solve the steady-state heat conduction problem governed by the Laplace equation in two-dimensional foam-like microstructures. These microstructures were idealized to an isotropic continuous matrix containing insulated circular voids. A typical model is illustrated in Figure 1*a*. A detail of the discretization strategy is depicted in Figure 1*b*. The model boundary is discretized using constant elements, which are clustered into a hierarchical multilevel quad-tree. The gray squares in Figure 1*b* are the leaves of a three-level quad-tree with at least 4 elements per leaf. The determination of the optimum number of elements per leaf will be discussed later in this section. Twelve expansion terms are used for the multipole expansion. The evaluations of all the integrals for the FMBEM matrix assembly are carried out analytically. The system of equations

is solved using a preconditioned GMRES algorithm from the public library Slatec [2011] with a convergence tolerance equal to 10^{-7}.

The FMBEM algorithm was calibrated for optimum performance and accuracy. To this end, the optimum element size for the model discretization and the number of elements per cell were investigated. This last parameter determines the extent of the near and far fields in the FMBEM collocation procedure [Liu and Nishimura, 2006]. The optimum element size was determined via a convergence analysis for a reference problem which was solved using a standard direct BEM solver. This reference problem was similar to that in Figure 1*a*. It consisted in a microstructure containing 100 holes of radius r=L/31 (L being the specimen dimension) arranged on a regular square-array with a void volume fraction f=0.327 (the ratio of the void volume to the total sample volume) . Boundary conditions were specified in order to induce a one-dimensional heat flux in the y-direction (see Figure 1*a*). The independency of the BEM solution with respect to the element size was explored in terms of the normalized flux Q/Q_0 through the sample. This was computed from the boundary solution using

$$\frac{Q}{Q_0} \cong \int_{i=1}^{P} q_i \, l_i, \tag{1}$$

where q_i and l_i are the heat fluxes and the element lengths of the P element, located along the top edge of the model (segment CD in Figure 1*a*). The symbol Q_0 stands for the flux for a void-free specimen. The number of elements was progressively increased and the results compared. Obtained results are plotted in Figure 2 using dark symbols. It was concluded from this analysis that a discretization using 4400 elements (40 elements per hole perimeter, 100 elements along the sample side) provides mesh-independent results.

The 4400-element mesh was used to tune-up the number of elements per cell. The number of elements per cell affects both, the quality of the solution and the efficiency of the algorithm. Figure 3 illustrates the error of the FMBEM results and the algorithm speed up with respect to the converged direct BEM solution as a function of the number of elements per cell. The error is presented in terms of the mean value and the standard deviation (error bars in the figure) of the element-by-element difference between the FMBEM and the direct BEM results. Results in Figure 3 show that if the number of elements per cell is greater than 10, the relative error reduces noticeably and its dispersion vanishes. The same trend can be observed in Figure 2, where the hollow symbols illustrate the convergence of the FMBEM results towards the direct BEM ones as the number of elements per cell increases. Similarly, the algorithm speed-up improves with the increment of the number of elements per cell, but it dramatically diminishes when this number is

beyond 200. This change in the tendency occurs when the size of the near field is too big, and thus the algorithm ends up with a configuration similar to that of the direct BEM (one may imagine, as the extreme case, a picture consisting in a single cell enclosing the complete model in the near field). Based on the above results and prioritizing accuracy over performance, the number of elements per cell was selected equal to 200. Furthermore, the algorithm performance using 200 elements per cell was investigated in terms of the model size. Obtained results are plotted in Figure 4. It can be observed that the speed up monotonously increases with the model size, performing, for the model sizes explored, up to 14 times faster than the standard BEM.

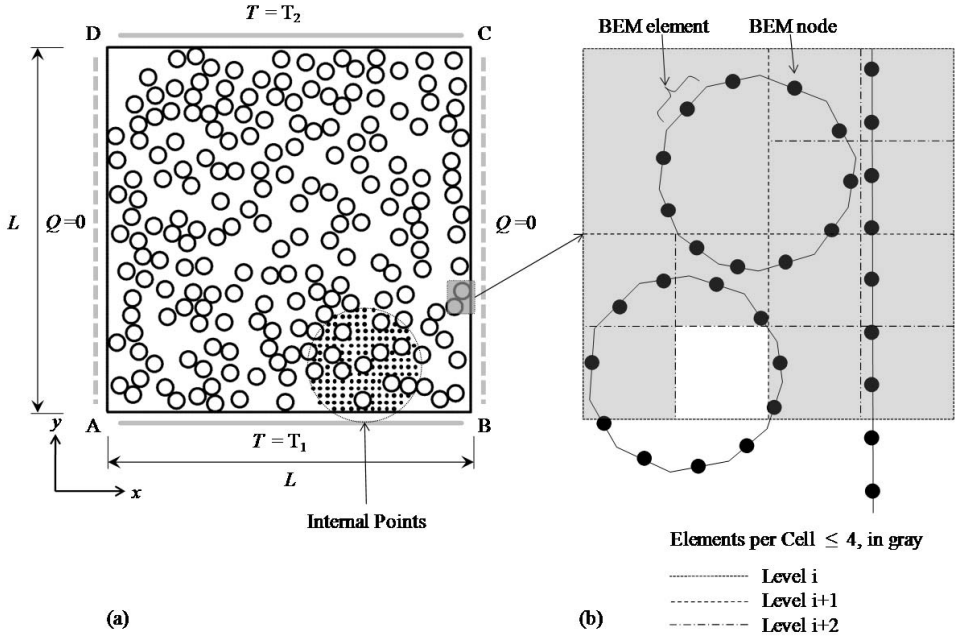

Figure 1: (*a*) FMBEM model of a representative volume element with a void volume fraction $f = 0.3$ (344 holes). (*b*) Detail of the FMBEM discretization depicting the hierarchical quad-tree clustering of the boundary elements.

3 Determination of the representative volume element size

In order to size the RVE a series of FMBEM analysis were performed for sets of samples with void volume fractions in the range $0 \leq f \leq 0.5$ and random distribution of the holes. The boundary conditions were set the same to those used in Section

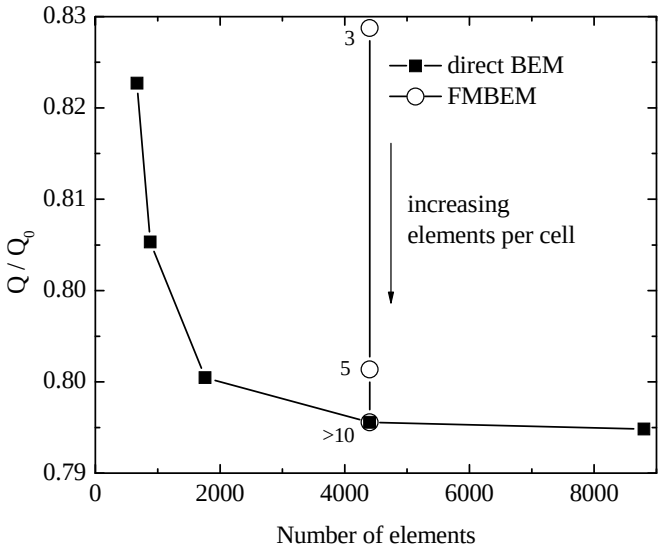

Figure 2: Normalized Flux as a function of the number of elements.

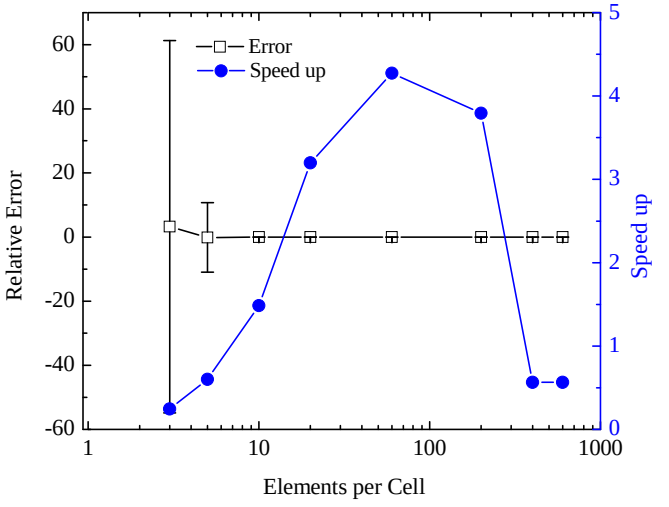

Figure 3: Relative error and FMBEM speed up vs. elements per cell.

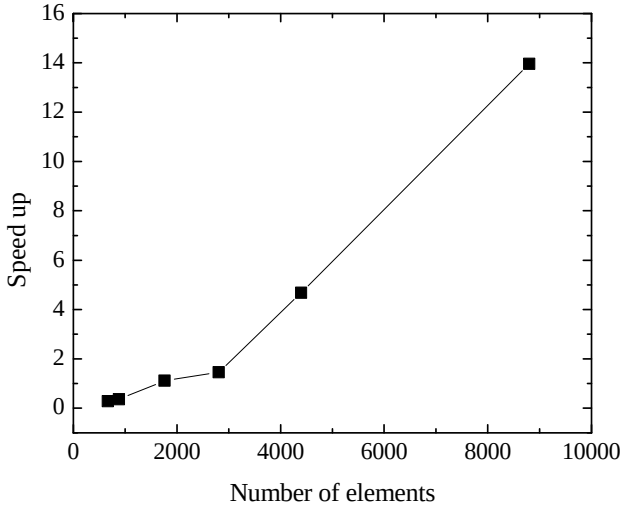

Figure 4: FMBEM speed-up as a function of the number of elements.

2 (see Figure 1*a*). The normalized ETC of the micro heterogeneous material was defined as $\alpha = k/k_0$, where k is the ETC of the micro heterogeneous material and k_0 is the thermal conductivity of a geometrically similar specimen without the holes. In this way, the normalized ETC can be computed using $\alpha = Q/Q_0$, this is, the same procedure introduced in equation 1.

The following number of holes per sample sequence was used to study the dependence of the effective responses on the sample size: 10, 30, 60, 100, 150, 200 and 300. Every computation was performed 20 times using models with different random distributions of the holes. In every case, the models were discretized using 40 elements along the hole perimeter (see Section 2). The resulting model sizes ranged from 504 to 13024 elements. It is interesting to mention that the solution of a single model like the one illustrated in Figure 1 using a laptop with a 3Ghz Pentium4 processor and 1Gb of RAM took around 53 seconds using the direct BEM formulation, whereas the FMBEM needed only of 13 seconds. This speed-up justified the implementation of the FMBEM for solving the $4\times7\times20$=560 models employed to size the RVE.

The mean and the standard deviation of the ETC results were calculated for each set of samples. The results are illustrated in Figure 5. It can be seen that the result dispersion diminishes as the number of holes per sample increases. Justified by the somewhat ad-hoc fact that for two successive enlargements of the number of holes the responses differed from one another, on average, by less than 0.5%, the

200-hole samples were selected as RVE for further analysis.

Further details and a comparison of the above ETC results with those of analytical and semi-empirical models can be found in Dondero et al (2011).

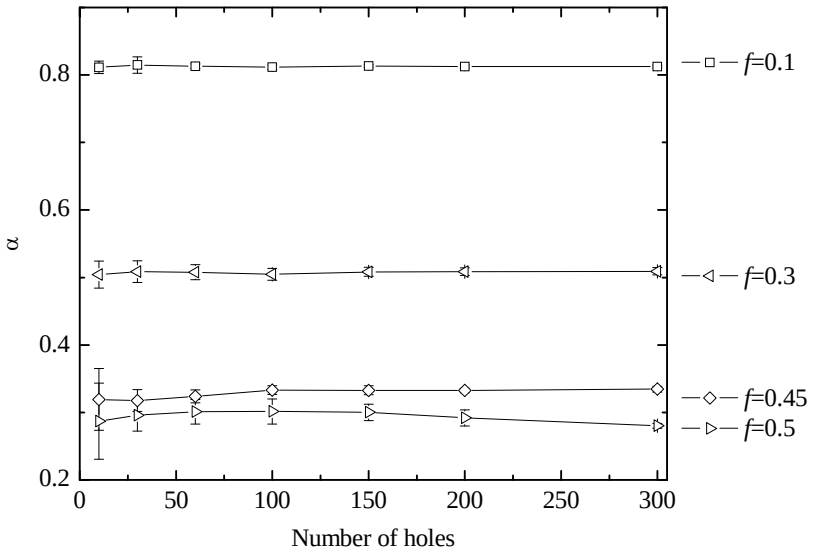

Figure 5: Effective thermal conductivity, $\alpha = k/k_0$, as function of the number of holes for a set of void volume fractions, f. Error bars indicate the standard deviation of the results computed for 20 different random distributions of the holes.

4 Optimization Using Genetic Algorithms

The GA code used in this work is a customization of PIKAIA, a self-contained, genetic-algorithm-based optimization subroutine developed by Charbonneau and Knapp.

The GA is used to optimize the spatial distribution of the void volume fraction along the y-direction in order to obtain an objective temperature field, $T(y)$, see Figure 6. To this end, the model domain is divided into n zones (parallel bands in Figure 6*a*) of equal length and over which the void volume fraction, $f(y)$, is linearly interpolated. The interpolation of the $f(y)$ is done in terms of m=n+1 discrete values, f_i , at the positions of the zone limits, see Figure 6*c*. The f_i are selected as design variables for the GA and they are codified into chromosomes

$$chromosome = f_1, f_2, \ldots, f_m. \tag{2}$$

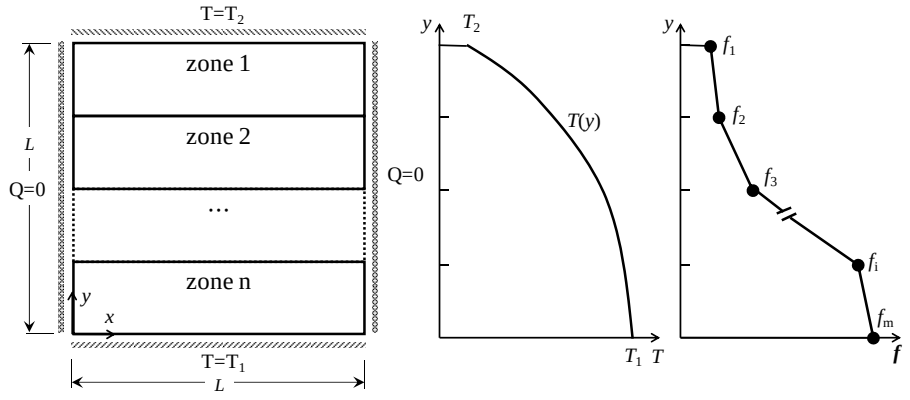

Figure 6: (*a*) Geometry with domain division, boundary conditions and dimensions; (*b*) objective temperature field; (*c*) piecewise linear interpolation of the void fraction along the RVE.

The chromosome representation is done in binary format.

The cost of the individuals (the cost function) is the deviation of the actual temperature field from the objective temperature field, $T(y)$. This is assessed using a least-squares scheme for the differences between the objective temperature field, $T(y)$, and the temperatures t_j computed for the set of the M internal points evenly distributed over the complete model domain:

$$cost\,(individual\ i) = \frac{\sqrt{\int_{j=1}^{M}\left[T\left(y_j\right)-t_j\right]^2}}{M}. \tag{3}$$

The internal point arrangement is depicted in Figure 1*a*. Note that the number of evaluation points cannot be guaranteed to remain constant during the optimization process due to change in the void volume fraction and the random distribution of the voids. So, the definition of the cost function in equation (3) implies an average.

The random distributions for the void positions are generated automatically using the rejection method with the distribution function given by the piece-wise definition for $f(y)$ [Press et al, 1992]. The models dimensions are always chosen bigger than the RVE size discussed in Section 3.

The critical issue in the implementation of the GA is the computational cost of the evaluation of the fitness function, which must be performed hundreds of even thousands of times for the solution of a single problem. In order to accelerate the computations a parallel version of the GA was developed. The GA was implemented to

run in parallel in a Beowulf PC cluster by incorporating MPI routines into PIKAIA. The parallel implementation of the GA is relatively simple due to natural independence of the cost function for each individual. The developed algorithm uses a master-slave scheme where the master node is in charge of the management of the GA (creating and populating each generation) and the slave nodes are dedicated to the evaluation of the cost of the individuals using the FMBEM solver. The scheme of the implementation is shown in Figure 7. The implementation was set up to run on a Debian-based GNU/Linux diskless cluster consisting of eight Intel Pentium 4 CPUs with 2 gigabytes of RAM each.

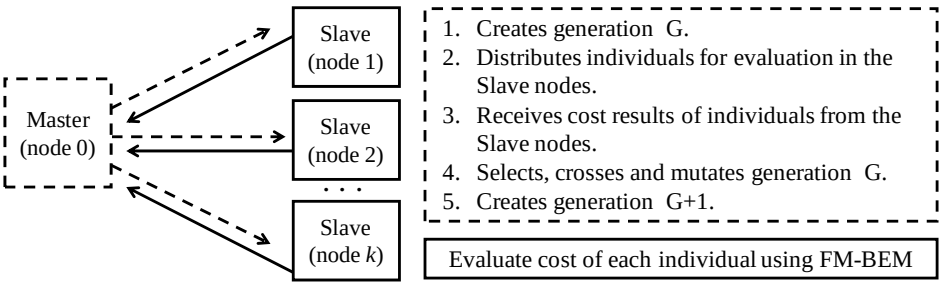

Figure 7: Parallel GA master/slave parallel implementation: master (broken lines) and slave (continuous lines) tasks and communication scheme (messages through MPI).

5 Material Designs

There are presented in this section the design of two materials with piece-wise constant and smooth continuous spatial variations of their normalized effective thermal conductivities, $\alpha[f(y)]$, respectively. The void volume fraction is allowed to vary within the range $0 \leq f(y) \leq 0.5$. The upper limit for $f(y)$ is the maximum value attainable using the sequential addition process for circular randomly-distributed holes of radius r separated by a minimum distance of $0.005r$ [Torquato, 2002].

Besides, and in order to guarantee that a solution for the optimization problem always exists, it is necessary to verify that the temperature field specified as objective function is feasible for the thermal conductivity values that can be attained within the void volume fraction $0 \leq f(y) \leq 0.5$. To this end, the Maxwell–Eucken 1 equation (ME1) [Wang et al, 2006] is used. The ME1 formula for the normalized ETC of a material consisting of a continuous matrix with a random dispersion of circular inclusions is

$$\alpha(f) = \frac{k_0 + k_d - (k_0 - k_d) f}{k_0 + k_d + (k_0 - k_d) f}, \tag{4}$$

where k_0 and k_d are the conductivities of the matrix and the inclusions respectively. Thus, by setting the conductivity for the matrix as k_0=1 and the conductivity of the inclusions (the voids) as k_d=0, it results from equation (4) that the range of normalized thermal conductivities associated to the void volume fraction $0 \leq f \leq 0.5$ is $1 \geq \alpha(f) \geq 0.333$.

5.1 Example 1: Material with piece-wise constant effective thermal conductivity

This first study case was designed as a benchmark problem. The goal is to test the ability of the optimization procedure to find the piece-wise constant solution of the void volume fraction, *f(y)*, that results in a bilinear piece-wise temperature field, $T(y)$. The problem set-up is depicted in Figure 6*a*, with the dimension L=60mm. The boundary conditions are T_2 = 100°C along the top edge of the specimen, and the flux q_1 = -1.4 W/mm^2 prescribed along the bottom edge. The lateral edges are insulated, this is, q = 0. Assuming that the bottom half of the specimen, $0 \leq y \leq 30$mm, has a void volume fraction f = 0.5, and that the void volume fraction in the top half, $30\text{mm} \leq y \leq 60\text{mm}$, is f = 0, the corresponding piece-wise linear temperature field for the objective function is

$$T(y) = 4.2\frac{^\circ C}{mm}y - 62^\circ\text{C} \quad 0mm \leq y \leq 30mm \tag{5}$$

$$T(y) = 1.2\ \frac{^\circ\text{C}}{mm}y + 28^\circ\text{C} \quad 30mm \leq y \leq 60mm.$$

It is easy to verify that the above objective function are the temperature solution for the problem consisting in a two-zone sample with normalized ETCs α_1 = 1 and α_2 = 0.333, the limiting values for the void volume fractions f=0 and f=0.5, respectively.

The optimization domain is divided into 8 zones, resulting in 9 design variables f_i. The chromosome is codified using 6 significant digits per design variable, what results in a chromosome length 9×6=54 genes (the number of design variables times the number of digits). The parameters for the GA are set as follows: population size 24 individuals, 50 generations, crossover probability 0.85, one point mutation mode with adjustable rate, initial mutation rate 0.005, minimum mutation rate 0.001, maximum mutation rate 0.0185, and full generational replacement reproduction plan with elitism. The setup of the GA follows the directions and suggestion in [Goldberg, 1999].

Figure 8 illustrates the evolution of the cost function in terms of the generation number for a typical GA solution. Results are plotted for the best individual (the most fitted) and the average cost for all the individuals in each generation. The

minimum is achieved after approximately 30 generations. It is worth noting that the convergence is not monotonous, but there are small fluctuations in the cost function as the optimization procedure progresses. These fluctuations are a consequence of the random nature of the microestructure geometry. The randomness in the microestructure geometry makes that two individuals generated using the same values for the design variables f_i will not be identical, and so, their costs will be different. This means that, even for the case when no improvement is made by the GA and the best fitted individual is kept for the next generation, the cost result could be improved or degraded. This behavior could be diminished by setting a tighter criterion when sizing the RVE, what would result in a bigger RVE (see Section 3). However, it must be noted that for the actual RVE size, the fluctuations in the fitness function are negligible with respect to the characteristic temperature of the example. Note that the maximum fluctuations in Figure 8 are of approximately 0.05°C, while the overall temperature difference along the sample 162 °C. This is, the fluctuation in the fitness function is only 0.04% the average mean temperature of the sample.

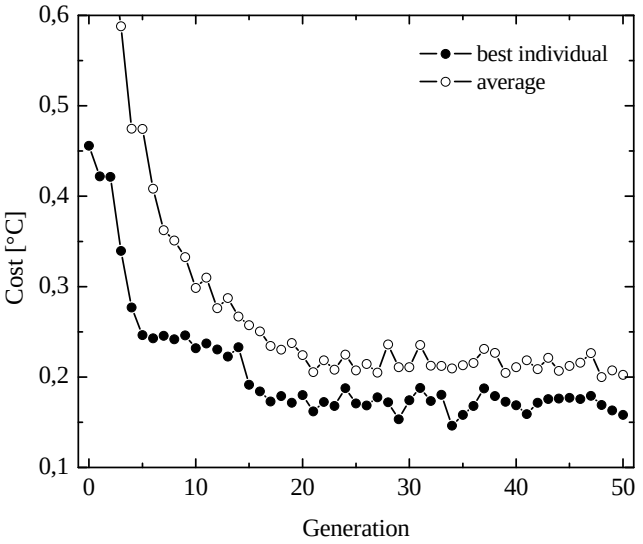

Figure 8: Fitness evolution for the first example: best-of-generation and average results.

The resultant optimized microstructure is shown in Figure 9*a* together with the contour plot of the temperature field. The void volume fraction solution, $f_i = 0.445$,

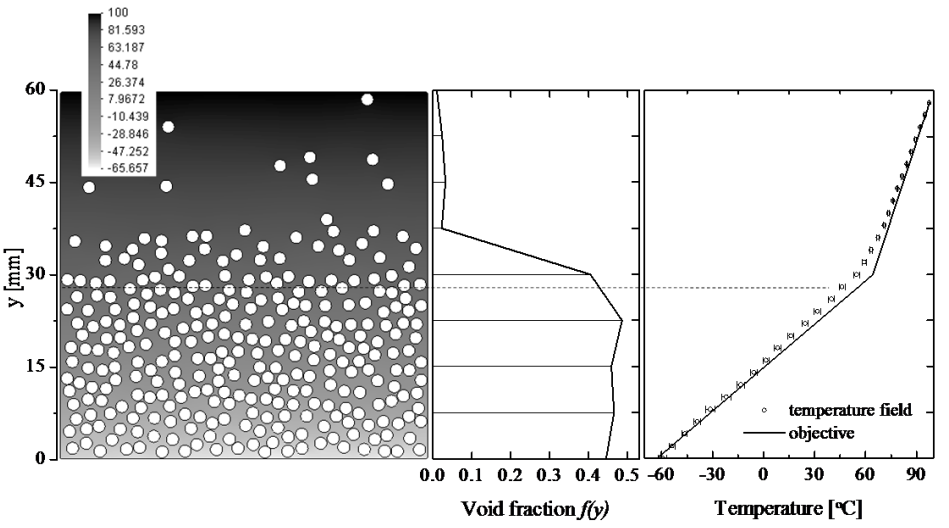

Figure 9: First example: (*a*) optimized microstructure with temperature contour plot, (*b*) void fraction solution, and (*c*) objective and resultant temperature fields.

0.465, 0.458, 0.486, 0.405, 0.022, 0.032, 0.023, 0.009, is plot in Figure 9*b* as a function of the *y*-position. Besides, the final temperature field is plotted in Figure 9*c*. The symbols in Figure 9*c* indicate the average value of the temperature results computed at the internal points located at the corresponding *y*-coordinate (see dotted line in Figure 9). The error bars indicate the dispersion of the results. It can be seen that the maximum difference between the objective function and the optimized result occurs in the neighborhood of $y = L/2 = 30$ mm, the position of the discontinuity in the ETC. As it was expected, the optimization procedure fails to exactly reproduce this abrupt variation of the ETC because it has been designed to produce continuous void volume fraction fields. However, it is worth noting that the transition from $f \cong 0.50$ to $f \cong 0$ occurs into a single design zone.

5.2 Example 2: Material with continuous variation in the thermal conductivity

It is proposed in this example to design a material with a smooth variation in the thermal conductivity in the *y*-direction. The specified temperature field for the objective function is

$$T(y) = 0.3133 + 1.989 \cdot y - 16.41 \cdot \tan^{-1}(0.0857 \cdot y - 2.56690)\,[^{\circ}\mathrm{C}]\,. \tag{6}$$

This objective function was devised to have a minimum gradient in the central portion of the optimization domain, and a maximum one at its ends, see Figure 10*c*.

The boundary conditions are similar to those of the Figure 6, with T_1=20°C and T_2=100°C are specified along the bottom and top edges of the sample respectively. The optimization procedure is used to obtain the void volume fraction $f(y)$ using an identical set-up to that of the first example.

Figure 10*a* depicts the resulting microstructure with the corresponding contour plot for the temperature field for one the best fitted individuals. Figure 10*b* presents the optimal void volume fraction solution, f_i = [0.477, 0.383, 0.319, 0.143, 0.059, 0.079, 0.295, 0.492, 0.292], and Figure 10*c* illustrates the comparison between the objective and the resultant temperature fields. It can be observed that there is an excellent agreement between the objective function and the resultant temperature field. This result was achieved after 20 generations.

The above result was further assessed by means of an analytical solution calculated using the comparison to Maxwell-Eucken 1 model [Wang et al, 2006]. The flux for the objective temperature field,

$$\mathrm{Q} = -\mathrm{k}(y)\,\frac{dT}{dy}, \tag{7}$$

is first computed for the temperature field in expression (6) assuming the minimum ETC at the bottom edge of the specimen

$$\mathrm{Q} = -\mathrm{k}(y)\,\frac{dT}{dy}\bigg|_{\mathrm{y}=0} = -0.333\frac{W}{^{\circ}\mathrm{C}\cdot mm}\cdot 1.804\frac{^{\circ}\mathrm{C}}{mm} = -0.601\frac{W}{mm^2}. \tag{8}$$

Then, since the flux must remain constant for every cross-section

$$\alpha(f) = \frac{k(y)}{k_0} = \frac{Q}{dT/dy} = -0.601\left[\frac{1.406}{(0.0857\ \mathrm{y} - 2.569)^2 + 1} - 1.989\right]^{-1}. \tag{9}$$

The above analytical estimation is plotted in Figure 11 together with that for the optimization analysis. It can be seen that both solutions exhibit the same behavior, with a maximum in the central zone of the sample, and minimum values at the sample ends. The optimized solution presents an increment in the conductivity at the position y=60 mm which is attributed to the random nature of the microstructure. However, the result in Figure 10*c* shows that this anomalous behavior does not affect the resultant temperature field.

6 Experimental validation

The numerical results obtained in the previous section were experimentally validated using ad-hoc designed experiments.

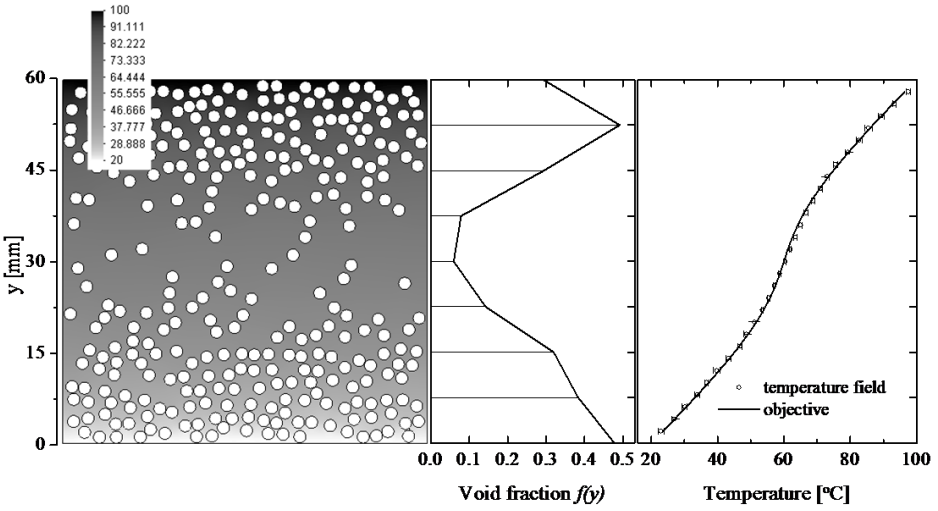

Figure 10: Second example: (*a*) optimized microstructure with temperature contour plot, (*b*) void fraction solution, and (*c*) objective and resultant temperature fields.

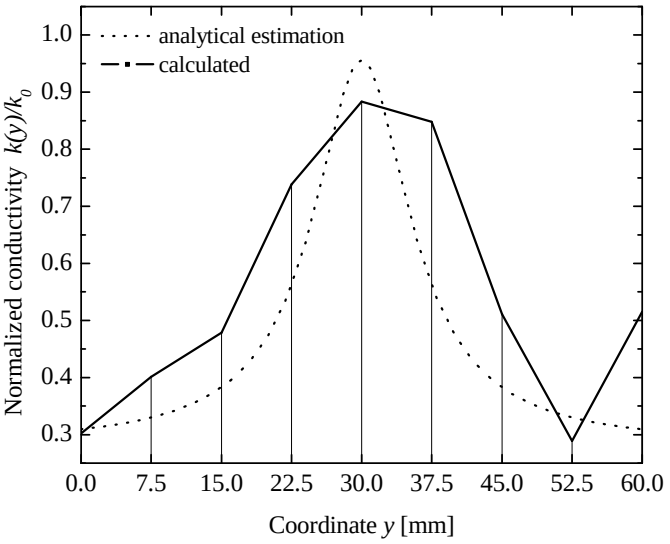

Figure 11: Analytical estimation and computed conductivity result for the second example.

Macroscopic specimens of the functionally-graded heat-conducting materials were constructed by machining circular holes in two highly-conductive 1100 AA-Grade aluminum 8mm thick plates. These designs are intended to approach the theoretical case of a highly-conductive continuous phase with non-conductive inclusions. Figure 12 illustrates the experimental setup. Temperatures labeled in the simulation as "$T = T_2$" and "$T = T_1$" were imposed in the physical experiment by means of a large-capacity heat source and a heat sink. The heat source was powered by a 400W electric resistance, while the sink consisted in a water cooling system and an electric resistance used to control the temperature. A 1/2" thick layer of alumina wool was placed beneath the bottom face and along the sides of the specimens in order to minimize convection and radiation heat losses. The holes in the specimens were plugged using alumina wool caps. Temperature maps were measured via thermal images taken using an infrared thermographic camera (Fluke Ti-30). The top face of the plate was painted matte black to maximize and homogenize the infrared specimen emittance. Figure 12 shows a typical infrared thermal image. Further details about the experiment setup can be found in the work by Dondero et al [2011].

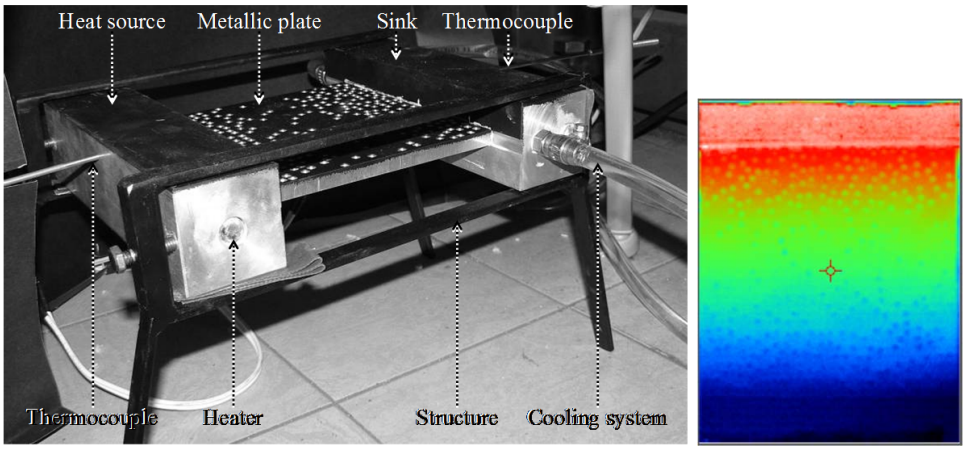

Figure 12: Left: Experimental setup. Right: thermal image showing the temperature map of the specimen.

Figures 13 and 14 depict the comparison between the experimental (gray-filled areas) and the FMBEM results. Error bars for the FMBEM results indicate the dispersion of the temperature results computed at the internal points located at the corresponding y-coordinate. It can be seen that with the only exception of the top and bottom edges of the specimen where the temperature values are boundary con-

ditions, the temperatures measured in the experiments are consistently lower than those computed using the FMBEM. This difference was attributed to the heat losses due to convection and radiation occurring in the experiment but not considered in the numerical model.

To ponder the heat-loss effects, a one-dimensional heat transfer problem was setup as follows:

$$k_0\ \alpha\left(f\left(y\right)\right)A_0\frac{dT}{dy} - h\,A\left(y\right)\left(T_{surf} - T_{envr}\right) - h_r\,A\left(y\right)\left(T_{surf} - T_{envr}\right) = 0 \tag{10}$$

where the first term accounts for the conduction heat transfer, and the second and third terms for the convection and radiation heat losses respectively. For the conduction term the ETC, $\alpha\left(f(y)\right)$, is computed using the Maxwell-Eucken 1 model with the void volume fraction data of the optimized materials, and k_0 = 237 W m^{-1} K^{-1} is the conductivity of the aluminum. The convection heat transfer coefficient is assumed constant along the specimen and set h = 4.35 W K^{-1} m^{-2} following the estimation formula $h = 0.38(\Delta T)^{0.25}$, where [$h$] = BTU ft^{-2} °C^{-1} hr^{-1}, and [ΔT] = °C as proposed for the design of cooling air fins [Mc. Adams, 1942]. The radiation transfer coefficient is calculated using $h_r = e\sigma\left(T_{surf} + T_{envr}\right)\left({T_{surf}}^2 + {T_{envr}}^2\right)$ where σ is the Stefan–Boltzmann constant, T_{surf} stands for the temperature on the specimen surface and T_{envr} is the environment temperature, which is set T_{envr} = 20°C. The value of the emittance is set e = 0.95 following Kreith and Kreider (1978).

Equation (10) was solved for both materials using a one-dimensional implicit finite differences iterative scheme with the plate length discretized into 100 elements. The effective area for the heat convection and radiation, $A\left(y\right)$, was computed for each element using $A\left(y\right) = A_0\left(1 - f(y)\right)$, where A_0 is the transverse area of the aluminum plate A_0 = 150mm × 8mm = 1200mm^2.

The temperature results considering the heat losses are plotted along the other results in Figures 13 and 14. It can be observed that their agreement with the experimental data is very good. The results for the temperature fields considering the effect of the heat losses lay within the dispersion of the experimental data for both materials. It is worth to remark that heat transfer and the emittance coefficients for the computation of the heat losses were retrieved from the literature, i.e. no data fitting was made to compute these values.

7 Conclusions

It has been introduced in this work an efficient numerical tool for the design of random micro-heterogeneous materials with functional-graded effective thermal conductivities (ETC). The optimization is carried using a parallel Genetic Algorithm

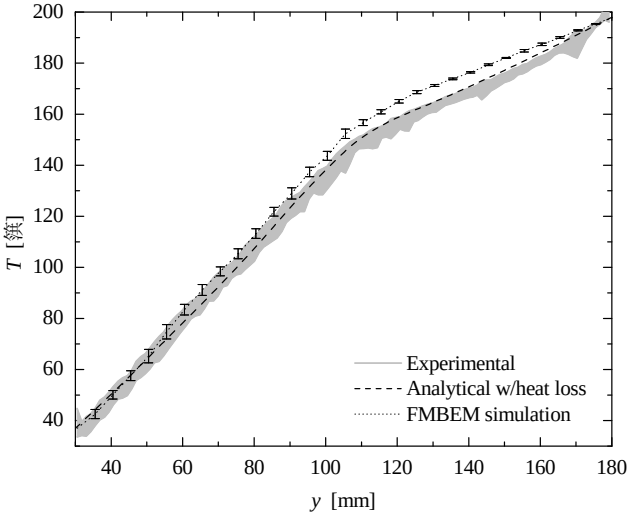

Figure 13: Temperature distribution along the plate for the first example.

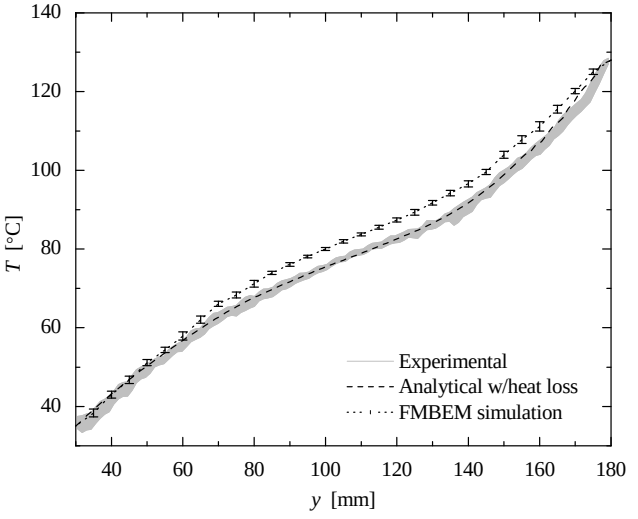

Figure 14: Temperature distribution along the plate for the second example.

(GA) and a Fast Multipole Boundary Element Method (FMBEM) for the evaluation of the cost function over representative volume elements (RVE).

The devised tool was tuned-up for the design of two-phase micro-heterogeneous functionally graded materials (FGM) consisting in a continuum matrix with non-conductive circular inclusions (insulated voids). It was found that in order to obtain mesh independent results, it is necessary to use at least 40 constant boundary elements for the discretization of each inclusion. A number of elements per cell equal to two hundred ensures a quality of the FMBEM results equal to that of a direct BEM. Speed-ups of up to 14 times with respect to a standard BEM solver were achieved for models using 8,800 elements.

Convergence and statistical analysis were performed in order to size the RVE. It was found that a sample containing at least 200 voids can be assimilated to RVEs for materials with a void volume fractions of up to f=0.5.

The effectiveness of the methodology has been demonstrated for two examples: a material with a piece-wise constant ETC, and a material with a smooth continuous spatial variation of the ETC. The optimization procedure succeeded to provide feasible microstructure topologies for both cases. The numerical predictions were experimentally validated by means of ad-hoc designed experiments, in which the temperature fields were measured by means of a thermographic camera. Very good agreement was found between the numerical and the experimental results.

It can be concluded that the proposed numerical procedure is effective for the design micro-heterogeneous functionally-graded thermal materials. Based on robust genetic and BEM algorithms, it is capable to account for the topological details of the material microstructure. Although the methodology was illustrated in this work to optimize the distribution of circular inclusions in one direction, it can be easily extended to deal with inclusions of arbitrary shape and orientation and multidimensional objective functions, this is, materials with graded properties in both the x- and y-directions.

Acknowledgement: This work has been partially supported by projects PICT07-1154 and PICT06-1359 of the Agencia Nacional de Investigaciones CientÃficas y Tecnológicas, the Universidad Nacional de Mar del Plata and the CONICET of Argentina.

References

Addams W.H. Mc. (1942): *Heat Transmissions*, pages 237-248, 2nd Edition, Mc Graw-Hill, New York, United States.

Aliabadi M.H. and Wrobel L.C. (2002): *The Boundary Element Method*, John

Wiley & Sons, Chichister, UK.

Birman V., Byrd L.W. (2007): Modeling and Analysis of Functionally Graded Materials and Structures, *Applied Mechanics Review*s, Vol. 60, pp. 195-216.

Charbonneau P., Knapp B. PIKAIA: Optimization (maximization) of user-supplied 'fitness' function ff over n-dimensional parameter space x using a basic genetic algorithm method. National Center for Atmospheric Research, Boulder CO 80307-3000, US. (`http://download.hao.ucar.edu/archive/pikaia`)

Chen J., Liu Z., Zou Z. (2002): Transient Internal Crack Problem for a Nonhomogeneous Orthotropic Strip, *Int. J. Engineering Science*, Vol 40, pp. 1761–1774.

Dondero M., Cisilino A.P., Carella J.M., Tomba J.P. (2011): Effective thermal conductivity of functionally graded random micro-heterogeneous materials using representative volume element and BEM, *International Journal of Heat and Mass Transfer*, Volume 54, Issues 17-18, August 2011, Pages 3874-3881, ISSN 0017-9310, DOI: `10.1016/j.ijheatmasstransfer.2011.04.041`.

Goldberg D.E. (1999): *Genetic Algorithms in search, optimization & machine learning*, Addison-Wesley, USA.

Kreith F. and Kreider J.F. (1978): *Principles of solar engineering*, pages 698-700, 1st Edition, Mc Graw-Hill, Washington, United States.

Liu Y.L., Nishimura N. (2006): The Fast Multipole Boundary Element Method for Potential Problems: A Tutorial, *Engineering Analysis with Boundary Elements*, Vol 30/5, pp 371-381.

Press W.H., Teukolsky S.A., Vetterling W.T., Flannery B.P. (1992): *Numerical Recipes in Fortran 77*, Second Edition. Cambridge University Press, Cambridge, UK.

Vandevender W.H., Haskell K.H. (2011): The SLATEC mathematical subroutine library, *SIGNUM Newsletter*, Vol 17/3, pp. 16-21, 1982. Available at `http://www.netlib.org/slatec/` (last visited in May 2011).

Wang J., Carson J.K., North M.F., Cleland D.J. (2006): A new approach to modeling the effective thermal conductivity of heterogeneous materials, *International Journal of Heat and Mass Transfer* 49, 3075–3083.

Sladek J., Sladek V., and Zhang Ch. (2003): Transient Heat Conduction Analysis in Functionally Graded Materials by the Meshless Local Boundary Integral Equation Method, *Computational Material Science*, Vol. 28, pp. 494–504.

Sutradhar A., Paulino G.H. (2003): The Simple Boundary Element Method for Transient Heat Conduction in Functionally Graded Materials, *Comput. Methods Appl. Mech. Eng.*, Vol. 193, pp. 4511–4539.

Sutradhar A., Paulino G.H., Gray, L.J. (2005): On Hypersingular Surface In-

tegral in the Symmetric Galerkin Boundary Element Method: Application to Heat Conduction in Exponentially Graded Materials, *Int. J. Numer. Methods Eng.*, Vol. 62, pp. 122–157.

Torquato S. (2002): *Random heterogeneous materials, microstructures and macroscopic properties*, Springer-Verlang New York, Inc., New York, NY.

Zohdi T.I., Wriggers P. (2005): Introduction to Computational Micromechanics, *Lecture Notes in Applied and Computational Mechanics*, Volume 20, First edition, Springer-Verlag, Berlin, cc. 1, 4, 9.

CMES: Computer Modeling in Engineering & Sciences

ISSN : 1526-1492 (Print); 1526-1506 (Online)

Journal website:
http://www.techscience.com/cmes/

Manuscript submission
http://submission.techscience.com

Published by
Tech Science Press
5805 State Bridge Rd, Suite G108
Duluth, GA 30097-8220, USA

Phone (+1) 678-392-3292
Fax (+1) 678-922-2259
Email: sale@techscience.com
Website: http://www.techscience.com
Subscription: http://order.techscience.com

CMES is Indexed & Abstracted in
Applied Mechanics Reviews; Cambridge Scientific Abstracts (Aerospace and High Technology; Materials Sciences & Engineering; and Computer & Information Systems Abstracts Database); CompuMath Citation Index; Current Contents: Engineering, Computing & Technology; Engineering Index (Compendex); INSPEC Databases; Mathematical Reviews; MathSci Net; Mechanics; Science Alert; Science Citation Index; Science Navigator; Zentralblatt fur Mathematik.